Table 3 Clinical characteristics of the patients according to the *MEN 1* gene mutation

Location	Pancreatic tumor	Pituitary tumor	Thymic tumor	Other tumors	Number of deaths and cause of death
Exon 2					
249_252delGTCT	5: Gas(1), Glu(1), Malig(1) Non(2)	3: PRL(3)	0	Meningioma (1)	2: Meningioma (1), pituitary crisis (1)
358_360delAAG	2: Non(2)	2: PRL(2)	0	Lung cancer (1)	0
133G > T	1: Non(1)	0	0	–	1: Liver metastases from gastrinoma
Exon 3					
455T > A	2: Gas(1) Non(1)	2: PRL(2)	0	–	1: Liver metastases from gastrinoma
512_520del GGGATGTCC	1: Non(1)	0	Unknown (1)	–	0
Intron 4					
784-9G > A	0	0	0	–	0
824 + 1G > A	0	0	0	–	0
Exon 6					
878delC	1: Non(1)	1: Non(1)	0	–	0
Exon 7					
959C > T	0	1: PRL(1)	0	–	0
955_956insT	0	0	0	–	0
914G > A	0	0	0	–	0
Exon 9					
1324C > T	0	0	0	–	0
Exon 10					
1546_1547insC	2: Gas(1) Non(1)	3: PRL(1), PRL and GH(1), ACTH(1)	0	Papillary carcinoma of the thyroid and osteomyelodysplasia (1)	0
1387G > T	1: Ins(1)	1: Non(1)	0	–	0
Large deletion	1: Gas(1)	0	2: carcinoid and cancer	–	1: Thymic cancer

Gas gastrinoma, *Glu* glucagonoma, *Ins* insulinoma, *PRL* prolactinoma, *GH* growth hormone producing adenoma, *ACTH* ACTH producing adenoma, *Non* non-functioning tumor, *Malig* malignant PNETs. (), number of patients; unknown, histological diagnosis was unknown

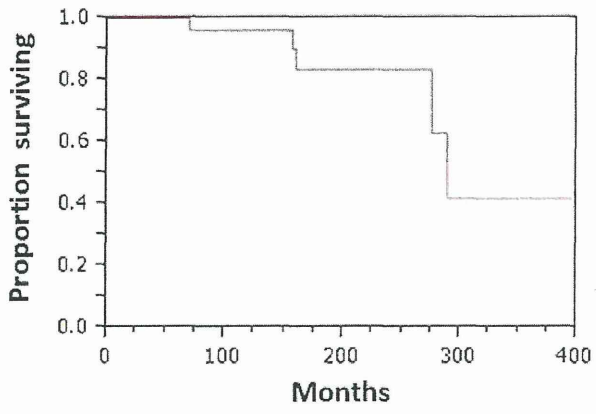

Fig. 1 Overall survival after initial parathyroidectomy in patients with MEN 1

living before the 1960s, whereas metastases of pancreatic carcinoids became the leading cause of death in the 1990s. Goudet et al. [16] also reported similar observations in MEN1 patients: the death rate due to GI hemorrhage was 14.5 % before the 1990s and fell to 2.8 % after the 1990s. Mortality due to tumor progression also changed from 47.8 % before the 1990s to 65.7 % thereafter [16]. Consequently, PNETs and carcinoids have been the predominant causes of death among patients with MEN1.

After the isolation of the *MEN1* gene, many investigators searched for genotype–phenotype or genotype–prognosis correlations. Kouvaraki et al. [17] reported that mutations in exon 2 are frequent in MEN1 patients with PNETs and mutations in exon 3 are frequent in those with thymic carcinoids. Ferolla et al. [18] reported that truncated

mutations are frequently present in patients with MEN1-associated thymic carcinoids. Kouvaraki et al. [17] found no relationship between genotype and prognosis.

The issues addressed in this retrospective study of MEN 1 patients were: (1) whether there are any genotype–phenotype correlations and (2) whether there are any prognostic predispositions depending on the *MEN1* genotype.

With regard to the first issue, we did not find any significant genotype–phenotype correlations. However, our experience is unique from several viewpoints. First, functional PNETs were observed in patients with *MEN 1* mutations in exons 2, 3 and 10 only. Second, thymic tumors were observed in patients with mutations in exon 3 and in the patient with the large deletion. Third, malignant diseases unrelated to MEN1, such as papillary thyroid carcinoma, lung cancer and osteomyelodysplasia, were observed only in patients with mutations in exons 2 and 10. Bartsch et al. [19] reported that patients with mutations in exons 2, 9 or 10 have a significantly higher rate of malignant PNETs (55 %) than those with mutations elsewhere (10 %). Kouvaraki et al. [17] reported that PNETs are frequently observed when the mutation is present in exon 2, whereas carcinoids are frequent when the mutation is in exon 10.

With regard to the second issue, MEN1-associated deaths were identified only among patients with mutations of exons 2 and 3 and in the one patient with a large deletion. However, it is premature to conclude that these mutations are specifically related to mortality. In fact, Vierimaa et al. [20] observed MEN1-related deaths in patients with mutations of exon 10.

Mortality associated with MEN1 in the present series was 16 %, which is quite different from figures reported previously [7, 14, 21]. One of the reasons for this difference may be advances in both knowledge and management of MEN1. In fact, in all of the cohort studies reported previously, the patients had been observed since the early 1900s.

The present study had several limitations. First, the study population included patients who had undergone parathyroidectomy. Such selection may have led to biased estimates of the phenotypic prevalence and disease-specific survival. Second, the number of patients (32) was too small to draw firm conclusions from the results. Third, the follow-up period was limited. Fourth, neither diagnostic nor follow-up examinations were uniform among the patients. The variation in work-up may have compromised the validity of the estimated disease frequency and prognosis.

In conclusion, no significant genotype–phenotype or genotype–prognosis correlations were observed in this study. The fact that the study involved a single institution may also have been a limiting factor. In addition, a longer follow-up period in the patients is needed. In 2008, researchers in Japan established a MEN study group, the "MEN Consortium of Japan," to construct a nationwide database of Japanese MEN patients. It is anticipated that this database will yield data on many unanswered questions related to MEN.

References

1. Marini F, Falchetti A, Del Monte F, Sala SC, Gozzini A, Luzi E, et al. Multiple endocrine neoplasia type 1. Orphanet J Rare Disease. 2006;1:38.
2. Brandi ML, Gagel RF, Angeli A, Bilezikian JP, Beck-Peccoz P, Bordi C, et al. Consensus: guidelines for diagnosis and therapy of MEN type 1 and type 2. J Clin Endocrinol Metab. 2001;86: 5658–71.
3. Larsson C, Skogseid B, Oberg K, Nakamura Y, Nordenskjold M. Multiple endocrine neoplasia type 1 gene maps to chromosome 11 and is lost in insulinoma. Nature. 1988;332:85–7.
4. Chandrasekharappa SC, Guru SC, Manickam P, Olufemi SE, Collins FS, Emmert-Buck MR, et al. Positional cloning of the gene for multiple endocrine neoplasia-type 1. Science. 1997;276: 404–7.
5. Agarwal SK, Kester MB, Debelenko LV, Hepper C, Emmert-Buck MR, Skarulis MC, et al. Germline mutations of the *MEN1* gene in familial multiple endocrine neoplasia type 1 and related states. Hum Mol Genet. 1997;6:1169–75.
6. Wermer P. Genetic aspects of adenomatosis of endocrine glands. Am J Med. 1954;16:363–71.
7. Dean P, van Heerden JA, Farley DR, Thompson GB, Grant CS, Harmsen WS, et al. Are patients with multiple endocrine neoplasia type prone to premature death? World J Surg. 2000;24:1437–41.
8. Erdheim J. Zur normalen und pathologischen Histologie der Glandula thyreoidea, parathyreoidea und Hypophysis. Beitr Pathol Anat. 1903;33:158–236.
9. Underdahl LO, Woolner LB, Black MB. Multiple endocrine adenomas: report of 8 cases in which the parathyroids, pituitary and pancreatic islets were involved. J Clin Endocrinol Metab. 1953;13:20–47.
10. Hai N, Aoki N, Matuda A, Mori T, Kosugi S. Germline *MEN1* mutations in sixteen Japanese families with multiple endocrine neoplasia type 1. Eur J Endocrinol. 1999;141:475–80.
11. Turner JJO, Leotleta PD, Pannett AAJ, Forbes SA, Bassett JHD, Harding B, et al. Frequent occurrence of an intron 4 mutation in multiple endocrine neoplasia type 1. J Clin Endocrinol Metab. 2002;87:2688–93.
12. Lemos MC, Takker RV. Multiple endocrine neoplasia type 1 (MEN1): analysis of 1336 mutations reported in the first decade following identification of the gene. Hum Mutat. 2008;29: 22–32.
13. Morelli A, Falchetti A, Martineti V, Becherini L, Mark M, Friedman E, et al. *MEN1* gene mutation analysis in Italian patients with multiple endocrine neoplasia type 1. Eur J Endocrinol. 2000;142:131–7.
14. Wilkinson S, Teh BT, Davey KR, McArdle JP, Young M, Shepherd JJ. Cause of death in multiple endocrine neoplasia type 1. Arch Surg. 1993;128:683–90.
15. Wilson SD, Krzywda EA, Zhu Y, Yen TWF, Wang TS, Sugg SL, et al. The influence of surgery in MEN-1 syndrome: observations over 150 years. Surgery. 2008;144:695–702.
16. Goudet P, Murat A, Binquet C, Cardot-Bauters C, Costa A, Ruszniewski P, et al. Risk factors and cause of death in MEN1 disease. A GTE (Group d'Etude des Tumeurs Endocrines) cohort study among 758 patients. World J Surg. 2010;34:249–55.

17. Kouvaraki MA, Lee JE, Shapiro SE, Gagel RF, Sherman SI, Sellin RV, et al. Genotype-phenotype analysis in multiple endocrine neoplasia type 1. Arch Surg. 2002;137:641–7.
18. Ferolla P, Falchetti A, Filosso P, Tomassetti P, Tamburrano G, Avenia N, et al. Thymic neuroendocrine carcinoma (carcinoid) in multiple endocrine neoplasia type 1 syndrome: the Italian series. J Clin Endocrinol Metab. 2005;90:2603–9.
19. Bartsch DK, Langer P, Wild A, Schilling T, Celik I, Rothmund N, et al. Pancreaticoduodenal endocrine tumors in multiple endocrine neoplasia type 1: surgery or surveillance? Surgery. 2000;128:958–66.
20. Vierimaa O, Ebeling TML, Kytola S, Bloigu R, Eloranta E, Salmi J, et al. Multiple endocrine neoplasia type 1 in northern Finland; clinical features and genotype-phenotype correlation. Eur J Endocrinol. 2007;157:285–94.
21. Doherty GM, Olson JA, Frisella MM, Lairmore TC, Wells SA, Norton JA. Lethality of multiple endocrine neoplasia type 1. World J Surg. 1998;22:581–7.

OPEN ACCESS Freely available online

PLOS ONE

Bone Marrow-Derived Microglia Infiltrate into the Paraventricular Nucleus of Chronic Psychological Stress-Loaded Mice

Koji Ataka[1], Akihiro Asakawa[2], Kanna Nagaishi[1], Kaori Kaimoto[2], Atsushi Sawada[3], Yuko Hayakawa[1], Ryota Tatezawa[1], Akio Inui[2], Mineko Fujimiya[1*]

1 Department of Anatomy, Sapporo Medical University School of Medicine, Sapporo, Japan, **2** Department of Psychosomatic Internal Medicine, Kagoshima University Graduate School of Medical and Dental Sciences, Kagoshima, Japan, **3** Department of Anesthesiology, Sapporo Medical University School of Medicine, Sapporo, Japan

Abstract

Background: Microglia of the central nervous system act as sentinels and rapidly react to infection or inflammation. The pathophysiological role of bone marrow-derived microglia is of particular interest because they affect neurodegenerative disorders and neuropathic pain. The hypothesis of the current study is that chronic psychological stress (chronic PS) induces the infiltration of bone marrow-derived microglia into hypothalamus by means of chemokine axes in brain and bone marrow.

Methods and Findings: Here we show that bone marrow-derived microglia specifically infiltrate the paraventricular nucleus (PVN) of mice that received chronic PS. Bone marrow derived-microglia are $CX_3CR1^{low}CCR2^{+}CXCR4^{high}$, as distinct from $CX_3CR1^{high}CCR2^{-}CXCR4^{low}$ resident microglia, and express higher levels of interleukin-1β (IL-1β) but lower levels of tumor necrosis factor-α (TNF-α). Chronic PS stimulates the expression of monocyte chemotactic protein-1 (MCP-1) in PVN neurons, reduces stromal cell-derived factor-1 (SDF-1) in the bone marrow and increases the frequency of $CXCR4^{+}$ monocytes in peripheral circulation. And then a chemokine (C-C motif) receptor 2 (CCR2) or a β_3-adrenoceptor blockade prevents infiltration of bone marrow-derived microglia in the PVN.

Conclusion: Chronic PS induces the infiltration of bone marrow-derived microglia into PVN, and it is conceivable that the MCP-1/CCR2 axis in PVN and the SDF-1/CXCR4 axis in bone marrow are involved in this mechanism.

Citation: Ataka K, Asakawa A, Nagaishi K, Kaimoto K, Sawada A, et al. (2013) Bone Marrow-Derived Microglia Infiltrate into the Paraventricular Nucleus of Chronic Psychological Stress-Loaded Mice. PLoS ONE 8(11): e81744. doi:10.1371/journal.pone.0081744

Editor: Jeffrey K. Harrison, University of Florida, United States of America

Received May 24, 2013; **Accepted** October 16, 2013; **Published** November 26, 2013

Copyright: © 2013 Ataka et al. This is an open-access article distributed under the terms of the Creative Commons Attribution License, which permits unrestricted use, distribution, and reproduction in any medium, provided the original author and source are credited.

Funding: This work was supported by Grants-in-Aid for Scientific Research of Japan Society for the Promotion of Science (#22590661 to KA). The funders had no role in study design, data collection and analysis, decision to publish, or preparation of the manuscript.

Competing interests: The authors have declared that no competing interests exist.

* E-mail: fujimiya@sapmed.ac.jp

Introduction

Microglia are innate immune-defense cells that react to brain infection and inflammation. During the embryonic stage, resident microglia migrate from the yolk sac into the brain where they reside for life [1,2]. Recently bone marrow-derived microglia have been reported to infiltrate into the brain parenchyma from the blood during brain injury, amyotrophic lateral sclerosis (ALS), multiple sclerosis, experimental autoimmune encephalomyelitis (EAE), and Alzheimer's disease [3–9].

The recruitment of bone marrow-derived cells into the brain in functional disorders caused by stress has not been well studied. We recently reported that chronically repeated foot-shock stress induced a massive infiltration of bone marrow-derived cells into the ventral hippocampus in mice [10]. However, to our knowledge, no studies have examined whether psychological stress can induce such infiltration into the CNS. Psychological stress originating from various somatosensory and nociceptive inputs is processed through higher centers of the brain and influences learning, emotional, and cognitive functions [11]. It is strongly related to anxiety, depression, and functional gastrointestinal disorders (FGIDs) including irritable bowel syndrome (IBS), functional dyspepsia (FD), and eating disorders [12,13].

The communication box (CB) method used in the present study is an experimental model to expose animals to psychological stress through visual, auditory, and olfactory stimuli produced by neighboring animals that receive electrical foot-shocks (Figure S1A). Psychological stress induced by CB has previously been shown to cause food intake suppression, anxiety, and depression [14–16]. We also recently

demonstrated that chronic psychological stress (chronic PS) induced by CB decreases antral motility and increases colonic motility in mice, which mimics FD and IBS [17].

The present study investigated the effects of chronic PS on the interaction between bone marrow-derived microglia and neurons, which has until now only been examined in the case of injury, inflammation, or neurodegenerative disease. Mechanisms for the recruitment of monocytes from bone marrow into the peripheral circulation and subsequent migration into specific brain nuclei were also examined. This study may give perspectives for the neuroregulatory effects of microglia in psychological stress reactions.

Methods

Animals

C57BL/6 male mice weighing 20–25 g at the start of the experiments were maintained under conditions of controlled temperature (22–24 °C), humidity (44–46%), and a 12-h light/dark cycle (light on 7:00–19:00). Food and water were available *ad libitum*. Mice were used once for each experiment. All animal experiments were approved by the Institutional Animal Care and Use Committee at Sapporo Medical University School of Medicine, Sapporo, Japan. We isolated bone marrow cells from tibias and femurs of adult GFP transgenic mice (C57BL/6 –Tg(CAG-EGFP), Japan SLC). These C57BL/6 EGFP transgenic mice have expression of enhanced green fluorescent protein (EGFP) directed to widespread tissues by the CMV-IE enhancer/chicken β-actin/rabbit β-globin hybrid promoter. Bone marrow cells (1×10^5 cells) were injected into the tail vain of recipient mice, which received whole-body irradiation of 9 Gy. To evaluate the effect of irradiation on infiltration of bone marrow-derived cells into brain, recipient mice were covered with a lead cap and received irradiation of 9 Gy. Transplanted recipient mice were maintained in cages covered by filter caps and given sterile water including 0.001 N HCl (pH 2.0) and sterile chow for two weeks to prevent infection. Eight to ten weeks after the bone marrow transplantation, the ratio of GFP positive cells in monocytes were examined in each mouse by FACS. Mice with chimeric ratio of larger than 90% were used in this study (Figure S1B and C). No difference was found in chimeric rates between mice with whole body irradiation and specific body irradiation with head protection.

Exposure to chronic PS by the CB

Eight to ten weeks after the bone marrow transplantation, mice were handled daily for 10 min by the same investigator for at least one week to prevent stress caused by subsequent experimental handling. The CB consists of nine compartments divided by transparent acrylic panels (Figure S1A; 16 × 16 × 40 cm, BS-CC01; BrainScience-idea, Osaka, Japan). Five electrical foot shock (FS) compartments have a grid floor made of stainless steel rods connected to an electric generator (BS-5ES; BrainScience-idea) and four compartments have a safety grid floor with no electrical connection. Five mice were placed individually in each of the FS compartments and received a 0.2 mA electric current of 10 s duration delivered randomly an average of twice per min for 60 min. Four more mice were placed individually in the psychological stress (PS) compartments with the safety floor. Mice in FS compartments cry and jump during 10s of electrical FS, and evacuate their bowels. Mice in PS compartments were surrounded by FS compartments on three sides, received visual, auditory, and olfactory stimuli from mice receiving electrical FS (Figure S1A). CB stress stimulation was performed for 1 h (10:00–11:00) daily and continued for five successive days, because we previously observed abnormal gastrointestinal motility caused by CB stimulation at fifth day of PS procedure [17]. Sham-treated controls were placed in PS compartments similar to the experimental group but with no stimuli.

Quantification of microglia infiltrating in the CNS

Immediately after stress-loading, mice were anesthetized with i.p. injection of sodium pentobarbital (50 mg/kg) and perfused through the left ventricle of the heart with phosphate-buffered saline (PBS), then 4% paraformaldehyde at the flow rate of 3 ml/min. Brains were cut into serial 20 μm coronal sections in a cryostat. We counted the number of GFP-positive cells at one side of the PVN in sections cut through hypothalamus at 200× magnification under confocal laser microscopy (A1; Nikon, Japan). The maximum number of GFP^+ cells from one section was obtained from each animal and used for analysis. PVN were distinguished according to Mouse Brain in Stereotaxic Coordinates written by Franklin & Paxinos.

Immunohistochemistry

Brain sections were incubated with a primary antibody for one to two days at a dilution of 1:500 for Ionized calcium-binding adapter molecule 1 (Iba-1, 019-19745; Wako Pure Chemical Industries, Osaka, Japan), 1:200 for Glial fibrillary acidic protein (GFAP, AB5541; Millipore, Billerica, CA), 1:100 for Monocyte Chemotactic Protein-1 (MCP-1, ab7202; Abcam, Boston, MA or SC-1784; Santa Cruz, Dallas TX), 1:100 for phosphorylated N-methyl-D-aspartate receptor (pNMDAR, 04-1064; Millipore), 1:100 for interleukin-1β (IL-1β, 503501; BioLegend), 1:250 for Protein gene product 9.5 (PGP9.5, AB5898, Millipore), 1:250 for NeuN (Neuronal Nuclei, ABN78; Millipore), or 1:25 for IL-1 receptor (AF771; R&D). Sections were then incubated for 2 h with Cy3, Cy5 or Alexa Fluoro 647-conjugated secondary antibody diluted 1:500. Nuclei were counterstained with 4',6-Diamidino-2-phenylindole dihydrochloride solution (DAPI, D523; Dojindo, Kumamoto, Japan). The image was observed using confocal laser microscopy (Nikon A1). In the quantification of $MCP\text{-}1^+NeuN^+$ cells or $MCP\text{-}1^+GFAP^+$ cells in PVN, we counted the number of $MCP\text{-}1^+NeuN^+$ cells or $MCP\text{-}1^+GFAP^+$ cells at one side of the PVN in sections cut through hypothalamus at 400× magnification under confocal laser microscopy (A1; Nikon). The maximum number of GFP^+ and $Iba\text{-}1^+$ cells from one section was obtained from each animal and used for analysis.

Isolation of microglia

Mice were anesthetized with i.p. injection of sodium pentobarbital (50 mg/kg) and perfused with sterile 0.1 M PBS for 5 min at the flow rate of 3 ml/min immediately after PS

exposure on day 5. Hypothalamic tissues taken from four mice were put together (n = 1) and dissociated to single-cell suspensions using the Neural Tissue Dissociation Kit (130-092-628; Miltenyi Biotec Inc., Germany) and Gentle MACS Dissociator (130-093-235; Miltenyi Biotec Inc.). Cells were washed with MACS buffer, and treated with MACS buffer containing FcR blocker (130-092-577; Miltenyi Biotec Inc.) then CD11b (microglia) MicroBeads (130-093-634; Miltenyi Biotec Inc.). CD11b-positive cells were isolated with a MACS MS column (130-042-201; Miltenyi Biotec Inc.), stained with anti-CD45 conjugated to APC (559864; BD Biosciences, Sparks, MD) and sorted with FACS Aria II (BD Biosciences). We used 12 mice to obtain the data (n = 4). The numbers of cells per 20000 total events in gate (1) or (2) were counted by FACS.

Quantitative real-time RT-PCR analysis

Total RNA was extracted from sorted microglia or isolated hypothalamus tissues using the RNeasy Micro Kit (74004; Qiagen, Hilden, Germany). cDNA was synthesized using SuperScript III First-Strand Synthesis System for RT-PCR (18080-051; Invitrogen, Carlsbad, CA) according to the manufacturer's instructions. Quantitative RT-PCR for the expression of CCR2, CX_3CR1, CXCR4, excitatory amino acid transporter 1(EAAT1), EAAT2, purinergic receptors (P2X4, P2X7, P2Y1, and P2Y12), IL-1β and tumor necrosis factor-α (TNF-α) on isolated microglia, and for the expression of MCP-1, stromal cell-derived factor 1(SDF-1), and fractalkine in hypothalamic tissues was performed on the ABI prism 7500 Sequence Detection System (Applied Biosystems, Foster City, CA) with Power SYBAR GREEN PCR Master Mix (4367659; Applied Biosystems). Relative mRNA expression was quantified by the $2^{-\Delta CT}$ method. Primer sequences are shown in Table S1.

The Length of axis of bone marrow-derived microglia

We measured the length of axis of $GFP^+Iba\text{-}1^+$ (bone marrow-derived microglia, BMDM) and $GFP^-Iba\text{-}1^+$ cells (resident microglia, RM) in chronic psychological stress-loaded and sham mice. The image was observed, and the length was measured using confocal laser microscopy and NIS Elements analysis software (Nikon).

Quantification of GFP^+CCR2^+ cells in peripheral blood and hypothalamus

Peripheral blood was sampled from chronic PS-loaded mice received the transplantation of bone marrow cells from GFP transgenic mice, and stained with anti-CCR2 antibody (ab32144, abcam) following to Alexa Fluor 647 conjugated secondary antibody (711-605-152, Jackson). The frequency was calculated from the following formula: the number of cells in the gate of GFP^+CCR2^+ divided by the number of cells in monocyte area gated by SSC-A and FFC-A on FACS. To count the number of $CCR2^+$ cells in hypothalamus of chronic PS-loaded and sham-treated mice, isolated $CD11b^+$ cells as mention above were stained with anti-CCR2 antibody followed by PE conjugated secondary antibody (12-4739, eBioscience, San Diego, CA), and then the numbers of GFP^+CCR2^+ and GFP^-CCR2^+cells per 10000 total events were counted by FACS.

Quantification of SDF-1 in bone marrow and GFP^+CXCR4^+ cells in peripheral blood

Femora from chronic PS-loaded mice without the irradiation were flushed out with Hanks' balanced salt solution. Cells were removed by centrifugation and the supernatant was assayed with an SDF-1 ELISA kit (C06021188, RayBiotech, Norcross, GA). Peripheral blood was obtained from chronic PS-loaded and sham-treated mice that received the transplantation of bone marrow cells from GFP transgenic mice. The blood samples were hemolyzed with RBC Lysis buffer (1045695, QIAGEN) and stained with anti-CXCR4 conjugated to APC (558644; BD Biosciences). The frequency was calculated from the following formula: the number of cells included in the gate of $CXCR4^+$ area divided by the number of cells in the monocyte area gated by side scatter pulse-area (SSC-A) and forward scatter pulse-area (FFC-A) on FACS.

The effects of antagonists on the accumulation of bone marrow-derived microglia

A CCR2 antagonist, RS102895 (R1903; Sigma, St Louis, MO), was administered orally with gavage (5 mg/kg), or a β_3-adrenergic blocker, SR59230A (1511; Tocris, Bristol, UK), was i.p. injected (1-mg/kg) daily 30 min before the PS stimulation. The sections of brain were prepared and stain with Iba-1 antibody following to Cy3-conjugated secondary antibody. We counted the number of GFP-positive cells at one side of the PVN in sections cut through hypothalamus at 200× magnification under confocal laser microscopy (A1; Nikon). The maximum number of GFP^+ and $Iba\text{-}1^+$ cells from one section was obtained from each animal and used for analysis.

Measurement of anxiety-like behavior

To evaluate the anxiety-like behavior in chronic PS-loaded mice we used the elevated plus-maze test according to the previous study [18]. Mice without irradiation and also without chimerism were administrated RS102895 (5 mg/kg) or saline (200 μl) orally with gavage daily 30 min before the psychological stress stimulation. After chronic psychological stress procedure on day 5 mice were put on the center of the elevated plus-maze apparatus and freely explore the maze for 5 min. We measured the time spent in open arms.

Statistical analysis

Data are expressed as means ± sem. Comparisons between two groups were performed using the two-tailed Student's t-test, while one-way analysis of variance (ANOVA) followed by Tukey's Multiple Comparison Test were used to compare groups of three or more. Differences were considered significant at $P < 0.05$.

Results

Chronic PS induces the infiltration of bone marrow-derived microglia into PVN of the hypothalamus

The number of GFP-positive cells in the PVN of PS-loaded mice was 1.2 ± 0.8 on day 1 and 4.5 ± 1.1 on day 2, which were not significantly different from those of sham-treated mice (2.6 ± 1.5 on day 1 and 4.3 ± 1.9 on day 2). On day 5, however, GFP-positive cells were significantly higher in number in PS-loaded mice (10.6 ± 0.5) compared with sham-treated mice (Figure 1A and B; $F_{5,36} = 4.43$, $P = 0.01$). GFP-positive cells in both chronic PS-loaded and sham-treated mice showed a ramified shape (Figure 1A), and were positively stained with Iba-1 but not GFAP (Figure 1C upper panels). GFP/Iba-1-double positive cells accumulated in the PVN, while GFP-negative/Iba-1-positive cells were diffusely scattered in the brain (Figure 1C lower panels). To evaluate the effects of whole body radiation on infiltration of bone marrow-derived cells, mice were received the specific body irradiation with head protection and bone marrow transplantation from GFP-Tg donors (Figure 1D). Eight to ten weeks after the bone marrow transplantation mice were exposed to psychological stress for five successive days using the CB. GFP-positive cells were increased in the PVN of psychological stress-loaded mice (Figure 1E; 3.8 ± 0.9 in stress-loaded mice and 0.1 ± 0.1 in sham mice, $P = 0.0022$), and stained with Iba-1 antibody (Figure 1F).

No difference was found in the number of GFP^+ cells in other area of brain between chronic PS and sham mice (Figure S2 and S3).

Bone marrow-derived microglia showed different mRNA expression from resident microglia

To avoid contamination of $CD11b^+CD45^+$ macrophages and monocytes, we sorted $CD11b^+CD45^{low}$ cells to isolate microglia [19] (Figure 2A). The number of GFP^+CD45^{low} cells was increased in chronic PS-loaded mice compared to sham-treated mice in both whole body radiation and radiation with head protection (Table 1, Figure 2A; P = 0.0042 and < 0.0001, respectively). There was no difference in the number of GFP^-CD45^{low} cells between chronic PS-loaded and sham-treated mice in both whole body radiation and radiation with head protection (Figure 2A).

We analyzed mRNA expression of proteins on GFP^+CD45^{low} and GFP^-CD45^{low} cells between chronic PS-loaded and sham-treated mice. No change was observed in the expression of any mRNA studied between chronic PS-loaded and sham-treated mice. However, a significant increase was detected in the mRNA expression of chemokine receptors, including CCR2 and CXCR4, in GFP-positive (bone marrow-derived) microglia compared with GFP-negative (resident) microglia in both chronic PS-loaded and sham-treated mice (Figure 2B; $F_{3,25} = 8.676$, $P < 0.0001$ and $F_{3,14} = 10.68$, $P = 0.0006$, respectively). The expression of IL-1β was also increased in GFP-positive microglia compared with GFP-negative microglia in both groups (Figure 2E; $F_{3,17} = 15.90$, $P < 0.0001$).

On the other hand, the expression of receptor CX_3CR1, EAAT1 and P2Y12 was decreased in GFP-positive microglia compared with GFP-negative microglia (Figure 2B, C, and D; $F_{3,12} = 21.97$, $P < 0.0001$, $F_{3,14} = 10.21$, $P = 0.0008$, and $F_{3,10} = 15.68$, $P = 0.0004$, respectively). TNF-α expression was also significantly decreased in GFP-positive microglia compared with GFP-negative microglia in both groups (Figure 2E; $F_{3,12} = 7.573$, $P = 0.0042$).

To evaluate the morphological differences between bone marrow-derived microglia and resident microglia, the length of axis of those cells was measured. No difference was found in morphology between bone marrow-derived and resident microglia (Figure 2 F).

Bone marrow-derived cells infiltrate the PVN through MCP-1/CCR2 chemotaxis in chronic PS-loaded mice

Because bone marrow-derived microglia highly express CCR2, we investigated whether MCP-1/CCR2 axis in brain is involved in the accumulation of bone marrow-derived cells in the PVN. The mRNA expression of MCP-1 in the hypothalamus was increased in chronic PS-loaded mice compared with sham-treated mice, although expression of SDF-1 and fractalkine (a CX_3CR1 ligand) in the hypothalamus was unchanged between the two groups (Figure 3A; P = 0.0046).

Increased expression of MCP-1 in the hypothalamus was confirmed by an immunohistochemical study. MCP-1 positive reaction was detected in both $NeuN^+$ neurons and $GFAP^+$ astrocytes in the PVN (Figure 3 B and C). The number of $MCP\text{-}1^+NeuN^+$ cells in the PVN was increased in chronic PS-loaded mice (24.1 ± 1.8) compared to sham-treated mice (10.7 ± 2.1, Figure 3B; P = 0.0005), while the number of $MCP\text{-}1^+GFAP^+$ cells in the PVN was unchanged between chronic PS-loaded mice (7.5 ± 0.5) and sham-treated mice (7.0 ± 0.5, Figure 3C).

In chronic PS-loaded mice the frequency of GFP^+CCR2^+ cells was increased in peripheral blood compared to sham-treated mice (Figure 3D, P = 0.0216). On the FACS analysis the number of GFP^+CCR2^+ in hypothalamus was increased in chronic PS-loaded mice compared to sham-treated mice (Figure 3 E; $F_{3,13} = 30.69$, $P < 0.05$). RS 102895 suppressed the accumulation of GFP-positive cells in the PVN induced by chronic PS (Figure 3F, $F_{2,10} = 12.45$, $P < 0.0019$). Furthermore, in measurement of anxiety-like behavior using the elevated plus-maze methodology on mice without irradiation as well as without bone marrow transplantation, RS102895 reversed the decrease in the time spent in open arms induced by chronic PS to the normal levels (Figure 3G; $F_{2,9} = 9.28$, $P = 0.0065$).

Bone marrow-derived cells egress from bone marrow into peripheral circulation through SDF-1/CXCR4 axis and β_3-adrenergic mechanisms in chronic PS-loaded mice

Because bone marrow-derived microglia highly express CXCR4, we investigated whether SDF-1/CXCR4 axis in the bone marrow is involved in the recruitment of bone marrow-derived cells in the peripheral circulation. The SDF-1 level in the bone marrow of chronic PS-loaded mice was significantly lower than in sham-treated mice (Figure 4A; P = 0.0126). Moreover, the percentage of GFP-positive $CXCR4^+$ peripheral blood monocytes was significantly higher in chronic PS-loaded

Figure 1

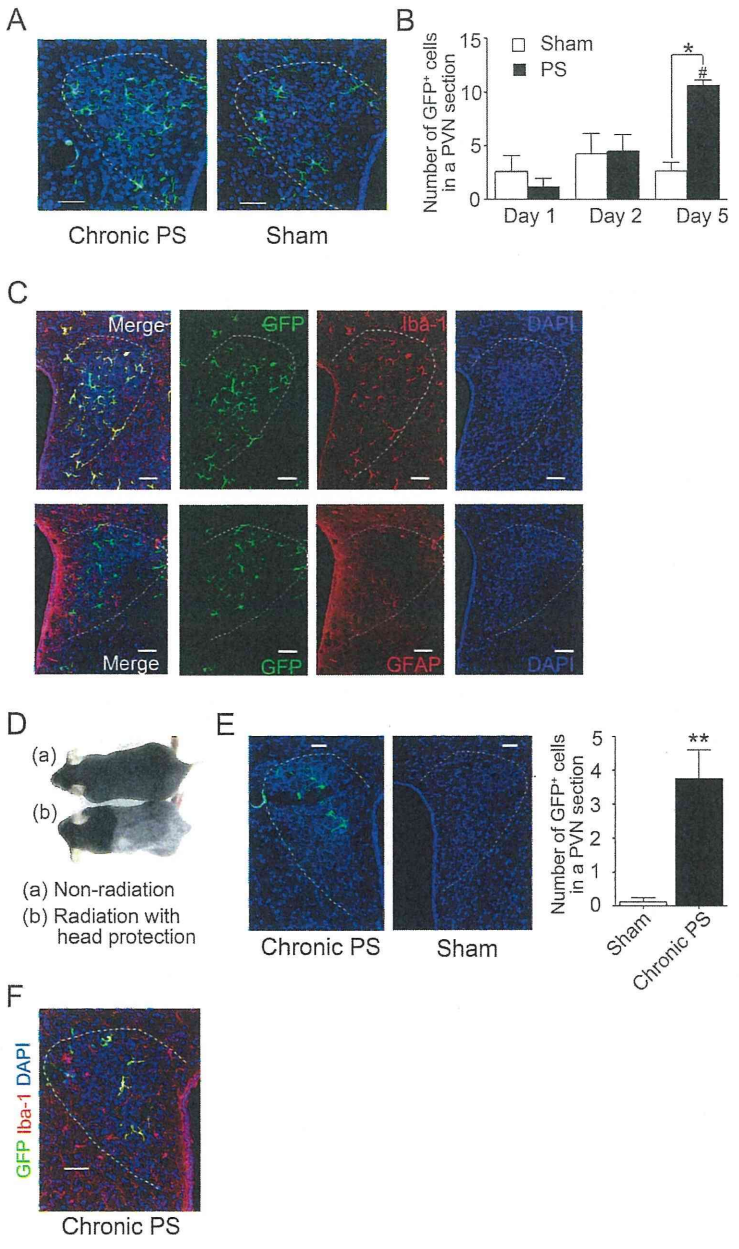

Figure 1. Chronic psychological stress (PS) increases the infiltration of bone marrow-derived microglia into the PVN. (A, B) After chronic PS-loading for five days, the numbers of GFP-positive cells (green) in the PVN were significantly increased compared with sham-treated mice. Data are expressed as mean ± sem (PS: n = 6–7, sham: n = 5–11). #$P < 0.05$ with ANOVA followed by Tukey's multiple comparison. *$P < 0.05$ with two-tailed Student's t-test. (C) GFP-positive cells (green) overlapped with Iba-1 (red) in PVN from chronic PS-loaded mice but did not overlap with GFAP (red) in PVN from chronic PS-loaded mice. (D) Photograph of mice received irradiation with head protection and non-irradiated mice. (E, F) After chronic PS-loading for five days, the number of GFP-positive cells (green) in the PVN of mice received the irradiation with head protection was significantly increased compared with sham-treated mice. Data are expressed as mean ± sem. **$P < 0.001$ for PS (n = 8) to sham (n = 4) with two-tailed Student's t-test. (G) GFP-positive cells (green) overlapped with Iba-1 (red) in PVN from chronic PS-loaded mice received the irradiation with head protection. PVN shown by dotted line. Scale bars: 50 μm.

doi: 10.1371/journal.pone.0081744.g001

Figure 2

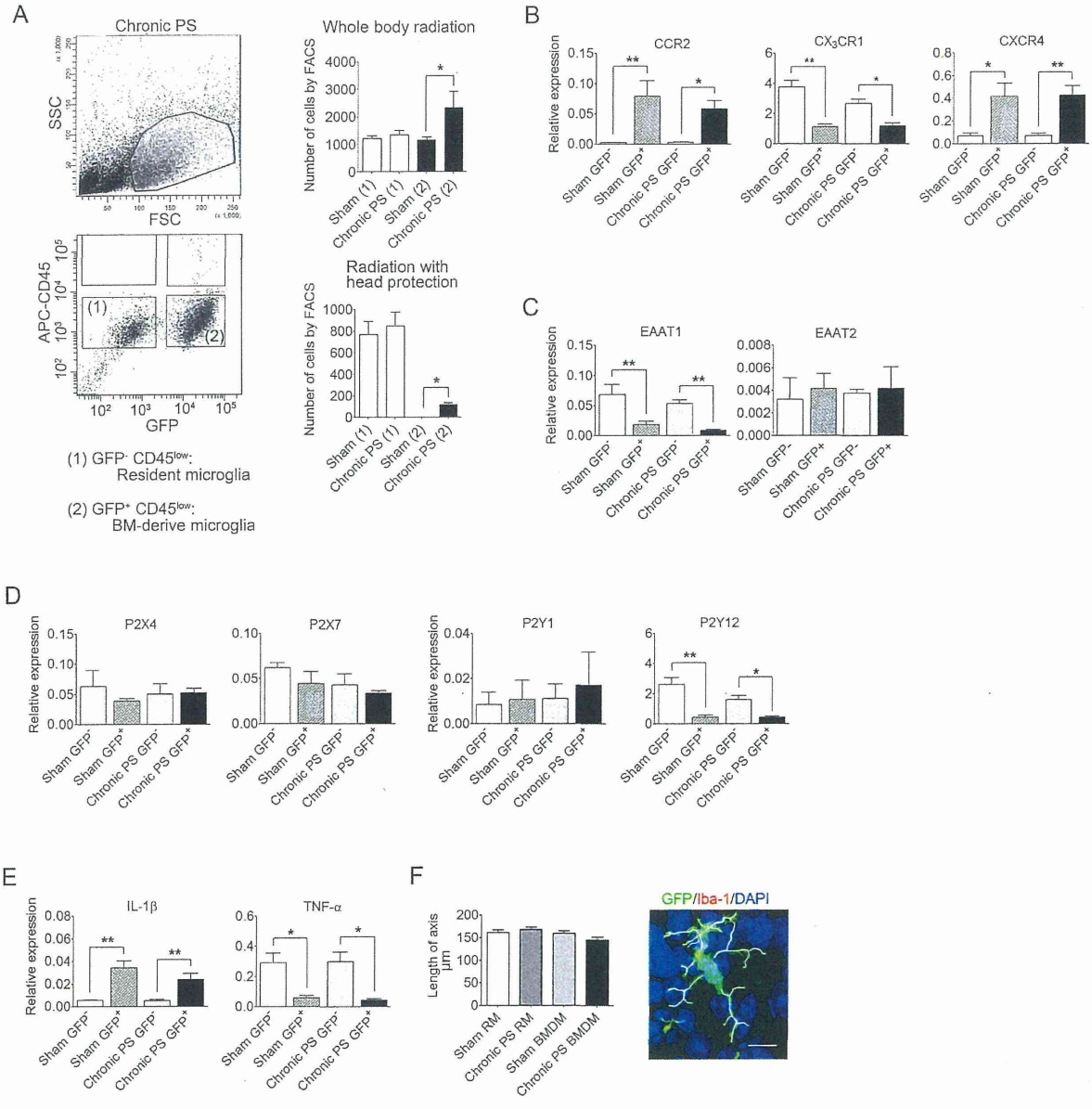

Figure 2. Isolation of bone marrow-derived microglia and resident microglia from hypothalamic tissue and comparison of expression of various molecules in chronic PS-loaded and sham-treated mice. (A) Representative FACS chart in chronic PS-loaded mice with whole body radiation and the number of isolated GFP$^-$CD45^{low} (resident microglia) and GFP$^+$CD45^{low} (bone marrow-derived microglia) from mice with whole body radiation and the radiation with head protection (n = 4–6). Total events in FACS were 20000. Data are expressed as mean ± sem. *P < 0.05 with two-tailed Student's t-test. (B–E) mRNA expression of chemokine receptors: CCR2 (n = 6–8), CX_3CR1 (n = 3–5), CXCR4 (n = 3–5) (B), exiting amino acid transporters: EAAT1 (n = 4–5), EAAT2 (n = 3–4) (C), purinergic P2X receptors: P2X4 (n = 3) and P2X7 (n = 3) and P2Y receptors: P2Y1 (n = 3), P2Y12 (n = 3–4) (D), IL-1β (n = 4–6) and TNF-α (n = 3–5) (E). (F) The length of axis of GFP$^+$Iba-1$^+$ microglia (bone marrow-derived microglia, BMDM) and GFP$^-$Iba-1$^+$ microglia (resident microglia. RM) in chronic PS-loaded and sham mice (n = 4). Scale bars: 10 μm. Data are expressed as mean ± sem. *P < 0.05, **P < 0.01 with ANOVA followed by Tukey's multiple comparison.

doi: 10.1371/journal.pone.0081744.g002

Table 1. The number of GFP$^-$CD45^{low} and GFP$^+$CD45^{low} cells.

Group (gate no.)	Whole radiation	Radiation with head protection
Sham (1)	1210 ± 111	768 ± 122
Chronic PS (1)	1342 ± 110	849 ± 126
Sham (2)	1165 ± 110	1 ± 1
Chronic PS (2)	2339 ± 564*	115 ± 20*

*. $P < 0.05$ v.s. Sham (2) ($n = 4–6$)

(1): GFP$^-$CD45^{low} cells, (2): GFP$^+$CD45^{low} cells

doi: 10.1371/journal.pone.0081744.t001

mice compared with sham-treated mice (Figure 4B; P = 0.0320).

To examine the involvement of β_3-adrenergic mechanisms in the pathways between chronic PS and the recruitment of bone marrow-derived cells from the bone marrow into the hypothalamus through peripheral blood, we administered SR59230A as a pretreatment. The SR59230A blocked the aggregation of GFP-positive cells in the PVN induced by chronic PS (Figure 4C; $F_{3,22} = 6.137$, $P = 0.0034$).

Bone marrow-derived microglia are IL-1β positive cells and exist in close vicinity to pNMDAR and IL-1 receptor positive neurons

By immunhistochemical overlap staining, IL-1β was stained in GFP$^+$ cells in the PVN from chronic psychological stress-loaded mice (Figure 5A). Those GFP$^+$ cells were located adjacent to pNMDAR positive (Figure 5B) and IL-1 receptor (IL-R) positive neurons (Figure 5C).

Discussion

Repeated exposure of PS to mice induces the recruitment of bone marrow derived-microglia into the PVN, which is an important locus for stress-induced functional disorders [20,21]. The number of GFP positive cells in PVN was increased in mice received whole body irradiation compared to mice received specific body irradiation with head protection, indicating that irradiation affected the permeability of BBB. In fact, in mice with head protection the number of GFP positive cells infiltrated into the brain was very small compared to those with whole body irradiation. However even under head protection, PS stimulated the migration of GFP positive cells in the PVN, those were positive for Iba-1. Therefore the results show that chronic PS stimulates accumulation of bone marrow-derived microglia in the PVN.

Bone marrow-derived microglia from mice with chronic PS-loaded and sham-treated mice have characteristics of CCR2$^+$CX$_3$CR1^{low} cells that are distinct from CCR2$^-$CX$_3$CR1^{high} resident microglia. This finding is consistent with a previous study which characterized bone marrow-derived cells infiltrating into the CNS in cases of EAE or CNS injury as Ly-6C^{high}CCR2$^+$CX$_3$CR1^{low} cells [4,7].

To isolate both bone marrow-derived microglia and resident microglia, we sorted CD11b$^+$ and CD45^{low} cells; therefore, sorted cells were distinct from the CD11b$^+$CD45^{high} perivascular macrophages, meningeal macrophages, resident monocytes or inflammatory monocytes [19]. Peripheral blood monocytes are classified into two subtypes, the inflammatory CD11b$^+$CX$_3$CR1^{low}CCR2$^+$ M1 monocytes, and the resident CD11b$^+$CX$_3$CR1^{high}CCR2$^-$ M2 monocytes [22]. According to chemokine receptor expression, bone marrow-derived microglia in the present study possess M1 monocyte characteristics, while resident microglia of the present study possess M2 monocyte characteristics. Previous reports showed that M1 monocytes activated by brain inflammation or brain injury secrete the pro-inflammatory cytokines TNF-α and IL-1β [23,24]. In the present study, bone marrow-derived microglia aggregated in the PVN expressed higher levels of IL-1β but lower levels of TNF-α compared with resident microglia.

Recently, several microglia phenotypes have been proposed in Alzheimer's disease, including M1, M2a, and M2c [25]. M1 represents 'classically activated' microglia that participate in inflammatory responses and were derived from "surveying microglia" by stimulation with TNF-α, IL-1β, and IL-6 [25]. M2a and M2c are 'alternative activated' microglia, which attenuate inflammatory responses and promote repair of tissue injury [25]. In Parkinson's disease, other subsets of microglia have been proposed, including classically activated microglia, chronically activated microglia, reactive microglia, and homeostatic microglia. The latter convert to classically activated microglia following acute inflammation, but convert to reactive microglia when expression of inflammatory cytokines is low, and chronic activated microglia when inflammation is prolonged [26]. As shown in previous studies, activated microglia can exert opposite effects on neurodegenerative reactions, for example, microbial pathogens may induce pro-inflammatory effects via toll-like receptors, while anti-inflammatory effects can be induced by apoptotic cells via the phagocytic receptor P2Y6 or the triggering receptor TREM2 [27]. In the present study, bone marrow-derived microglia in the hypothalamus resemble classically activated microglia because of their high expression of IL-1β, but there was no difference in morphology between bone marrow-derived and resident microglia, and their ramified shape matches that of surveying microglia. Therefore they are considered to be an alternative type of microglia from those previously classified.

The MCP-1/CCR2 chemokine axis is an important mediator of the migration of monocytes, memory T lymphocytes, and natural killer cells into affected areas in diseases such as multiple sclerosis, rheumatoid arthritis, type 2 diabetes, and Alzheimer's disease [28,29]. Our results show that chronic psychological stress stimulates the production of MCP-1 protein in PVN neurons and increases the mRNA expression of MCP-1 in the hypothalamus. Because bone marrow-derived cells express higher levels of the MCP-1 receptor CCR2 than resident microglia, they migrate into the PVN by the MCP-1/CCR2 axis. Indeed, aggregation of bone marrow-derived microglia in the PVN was blocked by peripheral administration of a CCR2 antagonist. Furthermore, a CCR2 antagonist was demonstrated to improve the anxiety-like behavior caused by chronic PS. Because these mice were not received irradiation

Figure 3

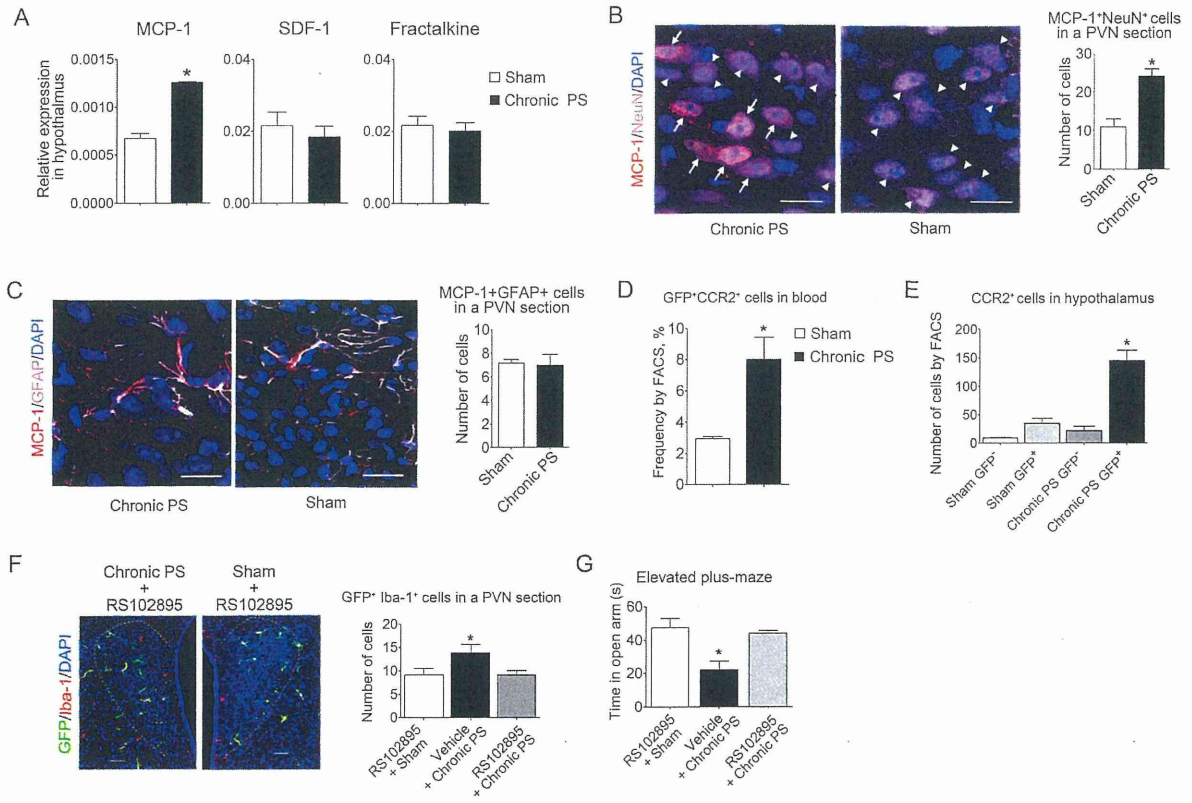

Figure 3. MCP-1/CCR2 axis in hypothalamus and peripheral blood, and effects of CCR2 blockade on the infiltration of bone marrow-derived microglia into the PVN and anxiety-like behavior induced by chronic PS. (**A**) mRNA expression of chemokines in hypothalamic tissue from chronic PS-loaded and sham-treated mice ($n = 4$). Data are expressed as mean ± sem. *$P < 0.05$ with two-tailed Student's *t*-test. (B) Immunofluorescence staining with MCP-1 (red) and NeuN (pink) in PVN from chronic PS-loaded and sham-treated mice. Arrows indicate MCP-1$^+$NeuN$^+$ cells and arrow heads indicate MCP-1$^-$NeuN$^+$ cells. Scale bars: 20 μm. Data are expressed as mean ± sem (n = 7). *$P < 0.05$ with two-tailed Student's *t*-test. (C) Immunofluorescence staining with MCP-1 (red) and GFAP (pink) in PVN from chronic PS-loaded and sham-treated mice. Scale bars: 20μm. Data are expressed as mean ± sem (n = 4–6). *$P < 0.05$ with two-tailed Student's t-test. (D) Frequency of GFP$^+$CCR2$^+$ cells in the peripheral blood obtained by FACS ($n = 4$–6). Data are expressed as mean ± sem. *$P < 0.05$ with two-tailed Student's *t*-test. (E) The number of CCR2$^+$ cells in the hypothalamus obtained by FACS ($n = 4$). Total events in FACS were 20000. Data are expressed as mean ± sem. *$P < 0.05$ with ANOVA followed by Tukey's multiple comparison. (F) Effects of a CCR2 antagonist, RS102895, on infiltration of bone marrow-derived microglia in PVN. PVN is shown by dotted line. Scale bars: 50 μm. Number of GFP-positive cells in a section including PVN is shown. (G) Effect of RS102895 on the anxiety-like behavior induced by chronic PS. Data are expressed as mean ± sem. *$P < 0.05$ with ANOVA followed by Tukey's multiple comparison ($n = 4$).

doi: 10.1371/journal.pone.0081744.g003

and not received bone marrow transplantation, the MCP-1/CCR2 axis in the brain was involved in the mechanism of the abnormal behavior induced by chronic PS.

The recruitment of bone marrow cells into the peripheral circulation is regulated by the SDF-1/CXCR4 interaction between bone marrow niche cells and hematopoietic stem cells [30–32]. A recent study showed that circadian oscillation originating from the suprachiasmatic nucleus in the brain stimulates β_3-adrenergic receptors on bone marrow stromal cells via sympathetic pathways [32]. Activation of β_3-adrenergic receptors on bone marrow stromal cells induces the reduction of SDF-1 production in the stromal cells, resulting in the decrease in the concentration of SDF-1 in the bone marrow. In the special microenvironments, niche, some stromal cells maintain the proliferation and differentiation of hematopoietic stem cells, which express CXCR4 on their surfaces. The

Figure 4

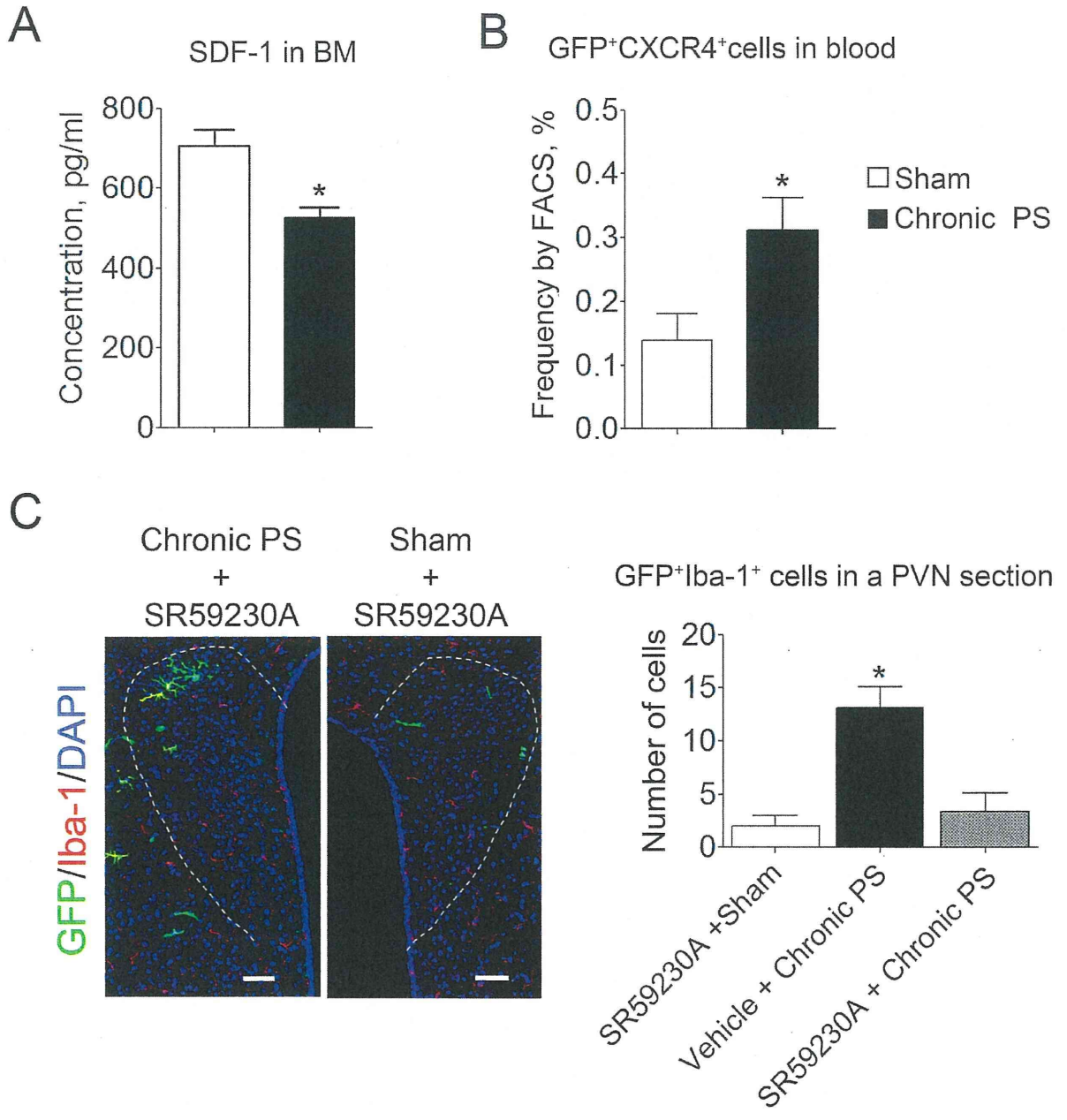

Figure 4. Expression of SDF-1 in the bone marrow and frequency of GFP$^+$CXCR4$^+$ cells in peripheral blood. Effects of β_3-adrenergic blockade on the infiltration of bone marrow-derived microglia in the PVN. (A) Chronic PS decreased the SDF-1 concentration in the bone marrow (n = 3–4) and increased the frequency of CXCR4$^+$ monocytes in the peripheral blood (n = 4–6). (B, C) β_3-adrenoceptor antagonist SR59230A blocks the infiltration of bone marrow-derived microglia in the PVN. Number of GFP-positive cells was counted in a section including PVN. Data are expressed as mean ± sem. *P < 0.05 (n = 3–11). PVN shown by dotted line. Scale bars: 50 μm.

doi: 10.1371/journal.pone.0081744.g004

Figure 5

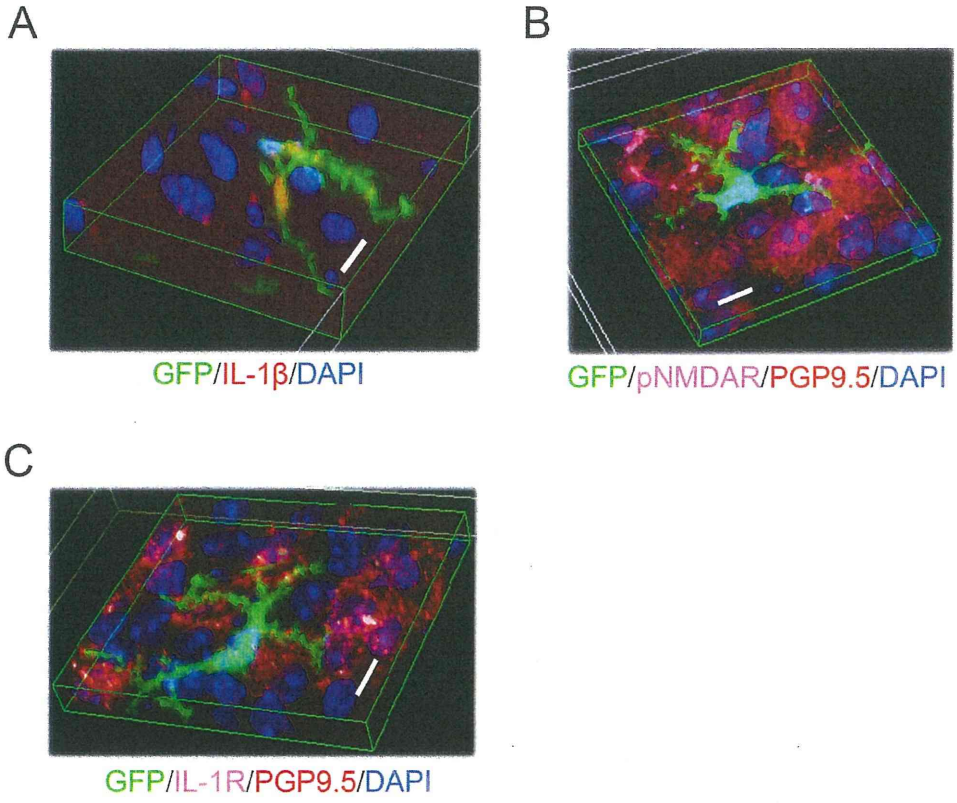

Figure 5. Three dimensional image of immunofluorescence staining of IL-1β, pNMDA receptor, and IL-1 receptor in PVN from chronic PS-loaded mouse. (A) GFP-positive cells (green) overlapped with IL-1β (red). (B, C) Positive reactions for pNMDAR (pink) and IL-1R (pink) detected on the membrane of neurons (red) adjacent to bone marrow-derived microglia (green) in PVN. Scale bars: 10 μm.

doi: 10.1371/journal.pone.0081744.g005

SDF-1/CXCR4 interaction is an important axis for the hematopoiesis. Therefore, the circadian oscillation stimulates the shedding of the differentiated cells from hematopoietic stem cells from the bone marrow and then increases the number of the differentiated cells in the peripheral blood [33]. In the present study, we showed that chronic psychological stress decreases the concentration of SDF-1 in bone marrow cells and increases the frequency of $CXCR4^+$ monocytes in the peripheral blood; furthermore β_3-adrenergic inhibition blocked the aggregation of bone marrow-derived cells in the PVN. These results suggest that chronic psychological stress stimulates sympathetic pathways and that activation of β_3-adrenergic receptors on the bone marrow cells induces a reduction in SDF-1 expression. This might then accelerate recruitment of monocytes from the bone marrow into peripheral circulations. Bone marrow niche cells constitute osteoblastic niche on endosteum and/or vascular niche on sinusoid, which regulate hematopoietic stem cells in differentiation and their recruitment into circulation [31,32]. Therefore chronic psychological stress may affect bone marrow niche functions via above mentioned pathways.

Bone marrow-derived microglia shown here highly express the pro-inflammatory cytokine IL-1β, which has been reported to be a key mediator in the alteration of synaptic signal transmission during injury, infection and diseases of the CNS [34,35]. In the spinal cord, microglia and astrocytes are activated by glutamate, substance P or ATP released from injured afferent presynaptic neurons [34]. These activated glia release various mediators including IL-1β and TNF-α and subsequently depolarize glutamatergic and GABAergic postsynaptic neurons [35]. In the hippocampus, on the other hand, IL-1β enhances both calcium signaling and excitatory postsynaptic currents through phosphorylation of NMDARs , which consists of glutamate-gated ion channels, via IL-1R; these pathways affect neuronal functions in neurodegenerative diseases [36–38] . The present study showed that bone

marrow-derived microglia from chronic psychological stress-loaded mice exist adjacent to neurons expressing pNMDARs and IL-1Rs. This indicates that bone marrow-derived microglia control neuronal transmission in PVN via activating phosphorylation of NMDARs through IL-1Rs under chronic PS conditions. IL-1β increases the permeability of blood-brain barrier and leads to the infiltration of leukocytes, macrophages and dendritic cells into brain parenchyma [39]. IL-1β expressing bone marrow derived monocyte could infiltrate into PVN.

The purinergic receptors P2X4, P2X7, P2Y6, and P2Y12 expressed on microglia are also involved in pain signaling in the spinal cord [40]. These receptors are activated by ATP, ADP or UDP released from injured primary afferent neurons, and activated microglia release PGE2, BDNF, TNF-α or IL-1β, which enhances depolarization of primary afferent neurons as well as inhibitory interneurons leading to neuropathic pain [40]. Microglia derived from $P2Y12^{-/-}$ mice were previously found to have no chemotaxic ability toward ATP and ADP [41]. The present results show that expression levels of P2X4, P2X7, P2Y6 and P2Y12 on bone marrow-derived microglia were similar or lower than those of resident microglia, suggesting that these purinergic pathways are not involved in the migration of microglia into specific brain nuclei.

In conclusion, we demonstrate that chronic psychological stress induces the aggregation of bone marrow-derived microglia in the PVN of mice and stimulates their recruitment into the circulation via the activation of β_3-adrenergic pathways and a subsequent reduction in SDF-1 expression on bone marrow niche cells (Figure 6). It is conceivable that bone marrow-derived microglia regulate neuronal transmission in the PVN as they attach to pNMDA receptor- or IL-1 receptor-expressing neurons.

Figure 6

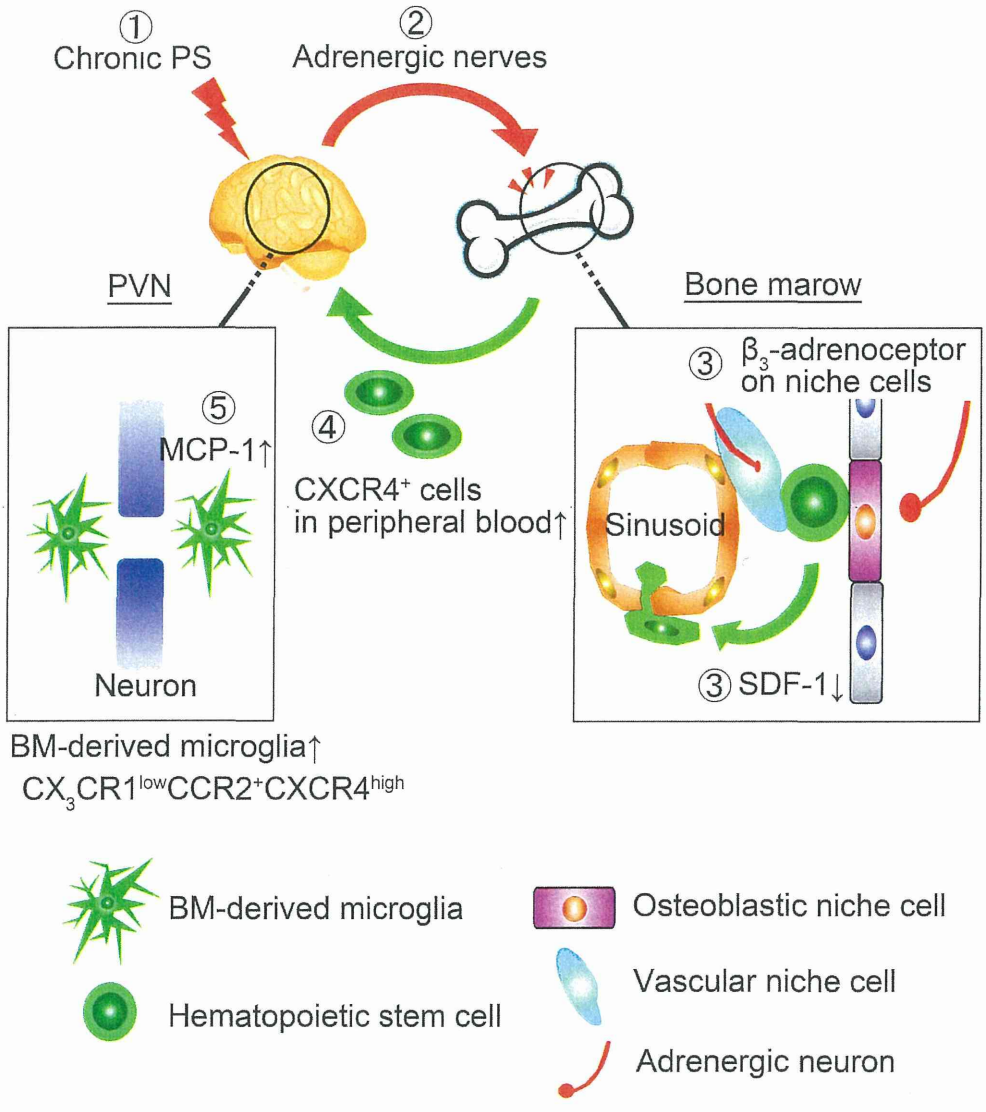

Figure 6. Schematic drawing of brain-bone marrow axis in chronic psychological stress conditions. When brain is exposed to chronic PS (1), the information is mediated to bone marrow through adrenergic nerves (2). Bone marrow niche cells innervated with sympathetic nerves decrease the expression of SDF-1 through β_3-adrenergic receptor (3). $CXCR4^{high}$ monocytes egress to peripheral circulation from the bone marrow by reduction of SDF-1 at the bone marrow niche (4). Neurons in the PVN express MCP-1 under chronic PS condition, then accelerate infiltration of $CCR2^{+}$ bone marrow-derived microglia into PVN (5).

doi: 10.1371/journal.pone.0081744.g006

Supporting Information

Figure S1. Communication box and chimeric ratio of peripheral blood from mice (A) Mice with bone marrow transplantation from GFP-Tg donors were placed in PS compartments and witnessed mice in the ES compartment receiving an electrical foot shock. (B, C) Chimeric ratio of mice received whole body irradiation (B) and specific body irradiation with head protection (C).
(TIF)

Figure S2. Representations of other area in brain of chronic psychological stress-loaded and sham mice. There are no differences of GFP$^+$ cells locations in other areas between the chronic psychological stress-loaded and the sham mouse.
(TIF)

Figure S3. The number of GFP$^+$ cells in hippocampus and central amygdala of chronic psychological stress-loaded and sham mice. We counted the number of GFP-positive cells in one side of the hippocampus (A) and central amygdala (B) within five successive sections at 200× magnification using confocal laser microscopy, and the maximum number of GFP$^+$ cells in a section was the representative data. Hippocampus and central amygdala were distinguished according to Mouse Brain in Stereotaxic Coordinates written by Franklin & Paxinos. In the amygdala the numbers of GFP$^+$ cells were counted in the area for 500 μm around of central amygdala.
(TIF)

Table S1. Primers for quantitative RT-PCR.
(DOCX)

Author Contributions

Conceived and designed the experiments: KA AA MF. Performed the experiments: KA KK YH RT AS. Analyzed the data: KA KN. Contributed reagents/materials/analysis tools: AA AI. Wrote the manuscript: KA MF.

References

1. Kettenmann H, Hanisch UK, Noda M, Verkhratsky A (2011) Physiology of microglia. Physiol Rev 91: 461–553. doi:10.1152/physrev.00011.2010. PubMed: 21527731.
2. Saijo K, Glass CK (2011) Microglial cell origin and phenotypes in health and disease. Nat Rev Immunol 11: 775–787. doi:10.1038/nri3086. PubMed: 22025055.
3. Beers DR, Henkel JS, Xiao Q, Zhao W, Wang J et al. (2006) Wild-type microglia extend survival in PU.1 knockout mice with familial amyotrophic lateral sclerosis. Proc Natl Acad Sci U S A 103: 16021–16026. doi:10.1073/pnas.0607423103. PubMed: 17043238.
4. Davoust N, Vuaillat C, Androdias G, Nataf S (2008) From bone marrow to microglia: barriers and avenues. Trends Immunol 29: 227–234. doi: 10.1016/j.it.2008.01.010. PubMed: 18396103.
5. Sharma S, Yang B, Strong R, Xi X, Brenneman M et al. (2010) Bone marrow mononuclear cells protect neurons and modulate microglia in cell culture models of ischemic stroke. J Neurosci Res 88: 2869–2876. PubMed: 20629187.
6. Prinz M, Mildner A (2011) Microglia in the CNS: immigrants from another world. Glia 59: 177–187. doi:10.1002/glia.21104. PubMed: 21125659.
7. Ajami B, Bennett JL, Krieger C, Tetzlaff W, Rossi FM (2007) Local self-renewal can sustain CNS microglia maintenance and function throughout adult life. Nat Neurosci 10: 1538–1543. doi:10.1038/nn2014. PubMed: 18026097.
8. Mildner A, Schmidt H, Nitsche M, Merkler D, Hanisch UK et al. (2007) Microglia in the adult brain arise from Ly-6ChiCCR2$^+$ monocytes only under defined host conditions. Nat Neurosci 10: 1544–1553. doi: 10.1038/nn2015. PubMed: 18026096.
9. Ajami B, Bennett JL, Krieger C, McNagny KM, Rossi FM (2011) Infiltrating monocytes trigger EAE progression, but do not contribute to the resident microglia pool. Nat Neurosci 14: 1142–1149. doi: 10.1038/nn.2887. PubMed: 21804537.
10. Brevet M, Kojima H, Asakawa A, Atsuchi K, Ushikai M et al. (2010) Chronic foot-shock stress potentiates the influx of bone marrow-derived microglia into hippocampus. J Neurosci Res 88: 1890–1897. PubMed: 20155811.
11. Kovács KJ, Miklós IH, Bali B (2005) Psychological and physiological stressors. In: T StecklerNH KalinJMH Reul. Handbook of stress and the brain, vol. 15. Elsevier: Amsterdam. pp 775–792.
12. Mönnikes H, Tebbe JJ, Hildebrandt M, Arck P, Osmanoglou E et al. (2001) Role of stress in functional gastrointestinal disorders. Evidence for stress-induced alterations in gastrointestinal motility and sensitivity. Dig Dis 19: 201–211. doi:10.1159/000050681. PubMed: 11752838.
13. Hauger RL, Risbrough V, Oakley RH, Olivares-Reyes JA, Dautzenberg FM (2009) Role of CRF receptor signaling in stress vulnerability, anxiety, and depression. Ann N Y Acad Sci 1179: 120–143. doi: 10.1111/j.1749-6632.2009.05011.x. PubMed: 19906236.
14. Ogawa N, Hara C, Takaki S (1993) Anxiolytic activity of SC-48274 compared with those of buspirone and diazepam in experimental anxiety models. Jpn J Pharmacol 61: 115–121. doi:10.1254/jjp.61.115. PubMed: 8096257.
15. Kuriyama H, Shibasaki T (2004) Sexual differentiation of the effects of emotional stress on food intake in rats. Neuroscience 124: 459–465. doi:10.1016/j.neuroscience.2003.12.012. PubMed: 14980395.
16. Abe H, Hidaka N, Kawagoe C, Odagiri K, Watanabe Y et al. (2007) Prenatal psychological stress causes higher emotionality, depression-like behavior, and elevated activity in the hypothalamo-pituitary-adrenal axis. Neurosci Res 59: 145–151. doi:10.1016/j.neures.2007.06.1465. PubMed: 17658641.
17. Ataka K, Nagaishi K, Asakawa A, Inui A, Fujimiya M (2012) Alteration of antral and proximal colonic motility induced by chronic psychological stress involves central urocortin 3 and vasopressin in rats. Am J Physiol Gastrointest Liver Physiol 303: G519-G528. doi:10.1152/ajpgi.00390.2011. PubMed: 22651925.
18. Nadal R, Escorihuela RM, Armario A (2006) The elevated plus-maze test of anxiety: methodological considerations. In: MJ Anderson. Task and techniques: A sampling of methodologies of the investigation of animal learning behavior and cognition. Nova Science Publishers Inc: NY. pp 25-37.
19. Prinz M, Priller J, Sisodia SS, Ransohoff RM (2011) Heterogeneity of CNS myeloid cells and their roles in neurodegeneration. Nat Neurosci 14: 1227–1235. PubMed: 21952260.
20. Bao AM, Meynen G, Swaab DF (2008) The stress system in depression and neurodegeneration: focus on the human hypothalamus. Brain. Res Rev 57: 531–553. doi:10.1016/j.brainresrev.2007.04.005.
21. Aguilera G (2011) HPA axis responsiveness to stress: implications for healthy aging. Exp Gerontol 46: 90–95. doi:10.1016/j.exger.2010.08.023. PubMed: 20833240.
22. Geissmann F, Jung S, Littman DR (2003) Blood monocytes consist of two principal subsets with distinct migratory properties. Immunity 19: 71–82. doi:10.1016/S1074-7613(03)00174-2. PubMed: 12871640.
23. Clausen BH, Lambertsen KL, Babcock AA, Holm TH, Dagnaes-Hansen F et al. (2008) Interleukin-1beta and tumor necrosis factor-alpha are expressed by different subsets of microglia and macrophages after ischemic stroke in mice. J Neuroinflammation 23: 5–46. PubMed: 18947400.
24. Henkel JS, Beers DR, Zhao W, Appel SH (2009) Microglia in ALS: the good, the bad, and the resting. J Neuroimmune Pharmacol 4: 389–398. doi:10.1007/s11481-009-9171-5. PubMed: 19731042.
25. Cameron B, Landreth GE (2010) Inflammation, microglia, and Alzheimer's disease. Neurobiol Dis 37: 503–509. doi:10.1016/j.nbd.2009.10.006. PubMed: 19833208.
26. Kosloski LM, Ha DM, Hutter JA, Stone DK, Pichler MR et al. (2010) Adaptive immune regulation of glial homeostasis as an immunization

strategy for neurodegenerative diseases. J Neurochem 114: 1261–1276. PubMed: 20524958.
27. Napoli I, Neumann H (2009) Microglial clearance function in health and disease. Neuroscience 158: 1030–1038. doi:10.1016/j.neuroscience.2008.06.046. PubMed: 18644426.
28. Deshmane SL, Kremlev S, Amini S, Sawaya BE (2009) Monocyte chemoattractant protein-1 (MCP-1): an overview. J Interferon Cytokine Res 29: 313–326. doi:10.1089/jir.2008.0027. PubMed: 19441883.
29. Hickman SE, El Khoury J (2010) Mechanisms of mononuclear phagocyte recruitment in Alzheimer's disease. CNS Neurol Disord Drug Targets 9: 168–173. doi:10.2174/187152710791011982. PubMed: 20205643.
30. Katayama Y, Battista M, Kao WM, Hidalgo A, Peired AJ et al. (2006) Signals from the sympathetic nervous system regulate hematopoietic stem cell egress from bone marrow. Cell 124: 407–421. doi:10.1016/j.cell.2005.10.041. PubMed: 16439213.
31. Ehninger A, Trumpp A (2011) The bone marrow stem cell niche grows up: mesenchymal stem cells and macrophages move in. J Exp Med 208: 421–428. doi:10.1084/jem.20110132. PubMed: 21402747.
32. Lilly AJ, Johnson WE, Bunce CM (2011) The haematopoietic stem cell niche: new insights into the mechanisms regulating haematopoietic stem cell behaviour. Stem Cells Int, 2011: 274564. doi:10.4061/2011/274564. PubMed: 22135682.
33. Méndez-Ferrer S, Lucas D, Battista M, Frenette PS (2008) Haematopoietic stem cell release is regulated by circadian oscillations. Nature 452: 442–447. doi:10.1038/nature06685. PubMed: 18256599.
34. Bradesi S (2010) Role of spinal cord glia in the central processing of peripheral pain perception. Neurogastroenterol Motil 22: 499–511. doi:10.1111/j.1365-2982.2010.01491.x. PubMed: 20236247.
35. Ren K, Dubner R (2010) Interactions between the immune and nervous systems in pain. Nat Med 16: 1267–1276. doi:10.1038/nm.2234. PubMed: 20948535.
36. Viviani B, Bartesaghi S, Gardoni F, Vezzani A, Behrens MM et al. (2003) Interleukin-1beta enhances NMDA receptor-mediated intracellular calcium increase through activation of the Src family of kinases. J Neurosci 23: 8692–8700. PubMed: 14507968.
37. Yang S, Liu ZW, Wen L, Qiao HF, Zhou WX et al. (2005) Interleukin-1beta enhances NMDA receptor-mediated current but inhibits excitatory synaptic transmission. Brain Res 1034: 172–179. doi:10.1016/j.brainres.2004.11.018. PubMed: 15713269.
38. Huang Y, Smith DE, Ibáñez-Sandoval O, Sims JE, Friedman WJ (2011) Neuron-specific effects of interleukin-1β are mediated by a novel isoform of the IL-1 receptor accessory protein. J Neurosci 31: 18048–18059. doi:10.1523/JNEUROSCI.4067-11.2011. PubMed: 22159118.
39. Shaftel SS, Carlson TJ, Olschowka JA, Kyrkanides S, Matousek SB et al. (2007) Chronic interleukin-1beta expression in mouse brain leads to leukocyte infiltration and neutrophil-independent blood brain barrier permeability without overt neurodegeneration. J Neurosci 27: 9301-9309. doi:10.1523/JNEUROSCI.1418-07.2007. PubMed: 17728444.
40. Tsuda M, Tozaki-Saitoh H, Inoue K (2010) Pain and purinergic signaling. Brain. Res Rev 63: 222–232. doi:10.1016/j.brainresrev.2009.11.003.
41. Haynes SE, Hollopeter G, Yang G, Kurpius D, Dailey ME et al. (2006) The P2Y12 receptor regulate s microglial activation by extracellular nucleotides. Nat Neurosci 9: 1512–1519. doi:10.1038/nn1805. PubMed: 17115040.

Am J Physiol Cell Physiol 305: C693–C703, 2013.
First published July 24, 2013; doi:10.1152/ajpcell.00400.2012.

CALL FOR PAPERS *Stem Cell Physiology and Pathophysiology*

Diabetes impairs the interactions between long-term hematopoietic stem cells and osteopontin-positive cells in the endosteal niche of mouse bone marrow

Hironori Chiba,[1] Koji Ataka,[2] Kousuke Iba,[1] Kanna Nagaishi,[2] Toshihiko Yamashita,[1] and Mineko Fujimiya[2]

[1]*Department of Orthopedic Surgery, Sapporo Medical University Faculty of Medicine, Sapporo, Japan, and* [2]*Department of Anatomy, Sapporo Medical University Faculty of Medicine, Sapporo, Japan*

Submitted 10 December 2012; accepted in final form 21 July 2013

Chiba H, Ataka K, Iba K, Nagaishi K, Yamashita T, Fujimiya M. Diabetes impairs the interactions between long-term hematopoietic stem cells and osteopontin-positive cells in the endosteal niche of mouse bone marrow. *Am J Physiol Cell Physiol* 305: C693–C703, 2013. First published July 24, 2013; doi:10.1152/ajpcell.00400.2012.—Hematopoietic stem cells (HSCs) are maintained, and their division/proliferation and quiescence are regulated in the microenvironments, niches, in the bone marrow. Although diabetes is known to induce abnormalities in HSC mobilization and proliferation through chemokine and chemokine receptors, little is known about the interaction between long-term HSCs (LT-HSCs) and osteopontin-positive (OPN) cells in endosteal niche. To examine this interaction, LT-HSCs and OPN cells were isolated from streptozotocin-induced diabetic and nondiabetic mice. In diabetic mice, we observed a reduction in the number of LT-HSCs and OPN cells and impaired expression of Tie2, β-catenin, and N-cadherin on LT-HSCs and β_1-integrin, β-catenin, angiopoietin-1, and CXCL12 on OPN cells. In an in vitro coculture system, LT-HSCs isolated from nondiabetic mice exposed to diabetic OPN cells showed abnormal mRNA expression levels of Tie2 and N-cadherin. Conversely, in LT-HSCs derived from diabetic mice exposed to nondiabetic OPN cells, the decreased mRNA expressions of Tie2, β-catenin, and N-cadherin were restored to normal levels. The effects of diabetic or nondiabetic OPN cells on LT-HSCs shown in this coculture system were confirmed by the coinjection of LT-HSCs and OPN cells into bone marrow of irradiated nondiabetic mice. Our results provide new insight into the treatment of diabetes-induced LT-HSC abnormalities and suggest that the replacement of OPN cells may represent a novel treatment strategy.

osteoblastic niche; Tie2; intrabone marrow-bone marrow transplantation

LONG-LASTING DIABETES IMPAIRS progenitor cell-dependent tissue repair, which is associated with the dysfunction of hematopoietic stem cells (HSCs) in the bone marrow. In type 1 diabetes, progenitor cell-dependent tissue repair is impaired, which is associated with endothelial or hematopoietic progenitor cell dysfunction in the bone marrow (19). The number of Lin^-, $Sca\text{-}1^+$, and $c\text{-}kit^+$ (LSK) hematopoietic progenitor cells in the bone marrow was previously demonstrated to be decreased in streptozotocin (STZ)-induced type 1 diabetic model of mice (7, 27). In the case of type 2 diabetes, the number of bone marrow-derived circulating $CD34^+$ cells was significantly reduced because of the reduced numbers of circulating endothelial progenitor cells. This has been proposed as a mechanism underlying the cardiovascular complications of diabetes (6). Diabetic mice were also shown to have diminished numbers of circulating LSK hematopoietic progenitor cells, leading to delayed wound closure (30).

The involvement of the stem cell niche or bone marrow microenvironment has been proposed as a means of understanding hematopoietic progenitor cell dysfunction (27). Specialized microenvironments (niches) support both self-renewal and the differentiation of HSCs, while their maintenance in a quiescent state is essential to protect them from stress and to sustain long-term hematopoiesis. HSCs are located in the trabecular endosteum (osteoblastic niche) or sinusoidal perivascular area (vascular niche; Ref. 5), the latter including CXCL12-abundant reticular (CAR) cells (26) or $nestin^+$ mesenchymal stem cells (22), which are characterized by high CXCL12 expression (5). In mouse models of diabetes induced by STZ or *db/db*, the CXCL12 mRNA levels in $nestin^+$ cells were reduced, and an impaired interaction between the CXCL12 expressed on $nestin^+$ cells and the HSC-expressed CXCR4 caused poor mobilization of hematopoietic cells after granulocyte colony-stimulating factor (GCSF) treatment (7, 22).

The osteoblastic niche appears to be more involved than the vascular niche in diabetic stem cell abnormalities, because diabetic mice showed significantly reduced numbers of osteoblastic but not $nestin^+$ cells (7). Osteoblasts secrete cytokines/chemokines, including GCSF; granulocyte-macrophage colony-stimulating factor (GM-CSF); macrophage colony-stimulating factor (M-CSF); interleukin (IL)-1, IL-6, and IL-7; and CXCL12, which support HSC survival and differentiation (23). They also express molecules that regulate the HSC numbers, including angiopoietin (Ang), thrombopoietin (TPO), Wnt, Notch, and osteopontin (OPN; Ref. 34), and adhesion molecules including N-cadherin, vascular cell adhesion molecule-1 (VCAM-1), intracellular adhesion molecule-1 (ICAM-1), and annexin II (23). The interaction of HSCs with osteoblastic niche cells through cell adhesion molecules and chemokines and their receptors maintains the balance between cell division/proliferation and quiescence (1).

We previously reported that diabetes induces an increase in the infiltration of bone marrow-derived cells in peripheral organs such as the liver, dorsal root ganglia, and kidney tubulo-interstitial space and that abnormal cell fusion between bone marrow-derived cells and parenchymal cells causes chromosomal abnormalities and accelerates apoptosis in diabetic

Address for reprint requests and other correspondence: M. Fujimiya, Dept. of Anatomy, Sapporo Medical Univ. School of Medicine, South 1, West 17, Chuo-ku, Sapporo 060-8556, Japan (e-mail: fujimiya@sapmed.ac.jp).

 0363-6143/13 Copyright © 2013 the American Physiological Society

animals (4, 9, 31, 36). These findings imply that diabetes primarily leads to a dysfunction of the osteoblastic niche, which subsequently disrupts HSC quiescence and then leads to increased abnormal bone marrow-derived cells, which induce diabetic complications. This hypothesis is supported by the fact that age-dependent hematopoietic dysfunction results mainly from abnormalities in osteoblastic niche cells (21). Mayack et al. (21) reported that young mouse-derived long-term reconstituting HSCs (LT-HSC) cocultured with aged mouse-derived osteoblastic niche cells showed a reduced capacity for hematopoietic reconstitution compared with the young mouse-derived LT-HSCs cocultured with young mouse-derived osteoblastic niche cells. Moreover, the exposure of normal LT-HSCs to aged osteoblastic niche cells is sufficient to worsen the LT-HSC function (21). However, no investigations have been performed to determine whether the exposure of abnormal LT-HSCs to normal osteoblastic niche cells can reverse the LT-HSC abnormalities.

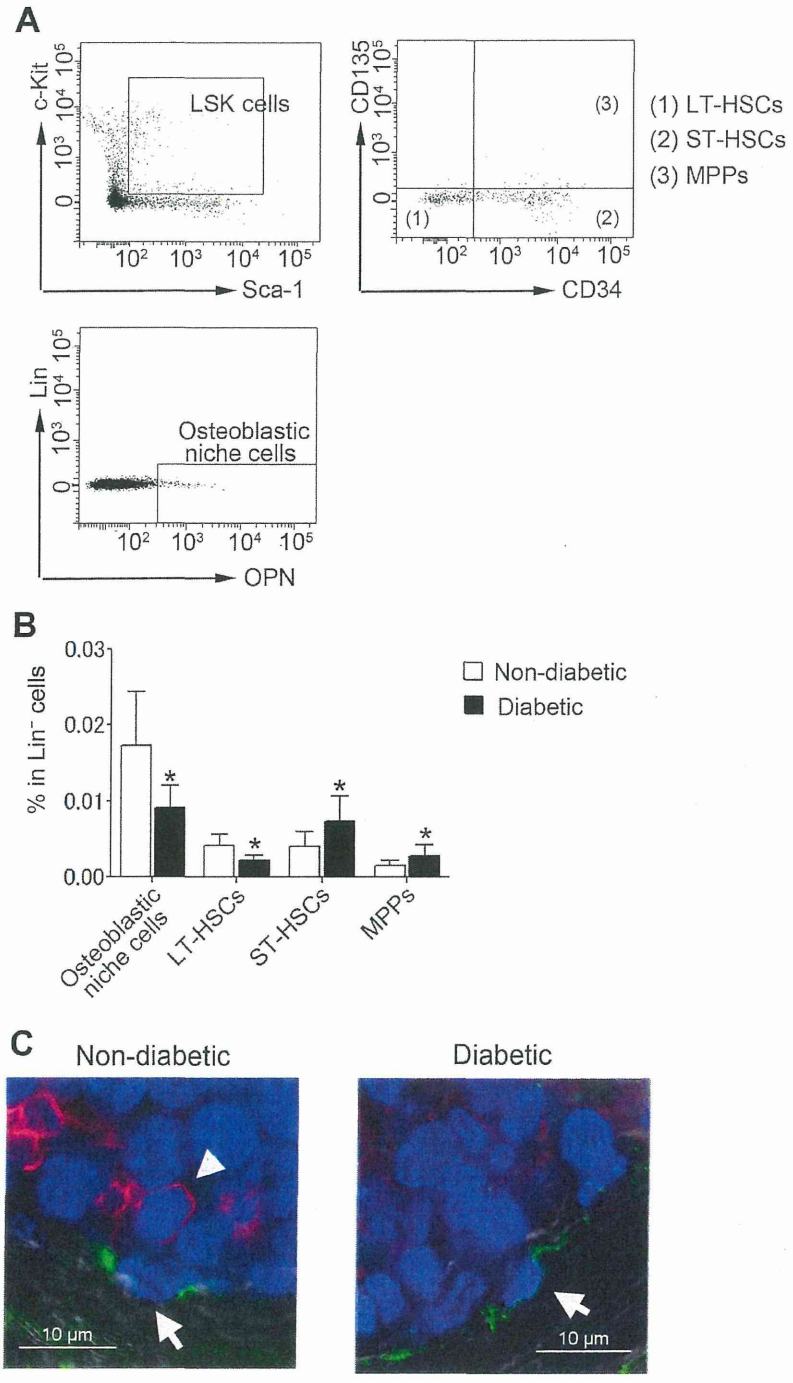

Fig. 1. Isolation of cells from bone marrow. *A*: representative FACS plot of the isolation of long-term hematopoietic stem cells (LT-HSCs; *1*), short-term hematopoietic stem cells (ST-HSCs; *2*), multipotent hematopoietic progenitors (MPPs; *3*), and osteoblastic niche cells. LSK, Lin^-, Sca-1^+, c-kit^+ cells. *B*: cell frequency in Lin^- bone marrow cells. *C*: localization of osteopontin-positive (OPN^+) osteoblastic niche cells (arrow, green) and $CD150^+$ LT-HSCs (arrowhead, red) in the bone marrow. Values are means ± SD for $n = 8$ mice. $^*P < 0.05$, compared with nondiabetic mice.

Therefore, in the present study, we performed in vivo experiments to examine whether diabetes induces the abnormal expression of molecules that are essential for maintaining the quiescence and reconstitution of HSCs in the bone marrow niche. Using in vitro coculture experiments, we also examined whether exposure of normal LT-HSCs to diabetic osteoblastic niche cells induced the abnormal expression of molecules on LT-HSCs seen in the in vivo experiments. We further examined whether the abnormal expression of molecules on diabetic LT-HSCs could be reversed following exposure to normal osteoblastic niche cells. Finally, these results obtained from in vitro studies were confirmed by intrabone marrow-bone marrow transplantation (IBM-BMT) with the replacement of osteoblastic niche cells and the effects on the LT-HSCs were examined.

MATERIALS AND METHODS

Animal studies. C57BL/6 male mice were purchased from the Sankyo Laboratory (Tokyo, Japan). Diabetes was induced by a single intraperitoneal injection of 150 mg/kg STZ dissolved in citrate buffer (pH 4.5) into 8- to 10-wk-old mice. Four weeks after the injection, the blood glucose levels were assayed, and mice with blood glucose concentrations >400 mg/dl were used in the present study. Nondiabetic control mice were injected with 100 μl of vehicle. All animal experiments were approved by the Animal Use Committee of Sapporo Medical University, Sapporo, Hokkaido, Japan.

Flow cytometry. LT-HSCs and osteoblastic niche cells were sorted as LSK $CD135^-$ $CD34^-$ cells and Lin^- OPN^+ cells, respectively (21). The femora and tibiae of four mice treated with vehicle or STZ were crushed and digested at 37°C for 1 h with Hanks' buffered saline including 0.25% trypsin, 1 mM EDTA (25200; Life Technologies, Grand Island, NY), and 0.1% collagenase (034–10533; WAKO, Osaka, Japan). Cells were washed with phosphate-buffered saline (pH 7.5) containing 2% FCS and were filtered through a 40-μm cell strainer filter (BD Biosciences, Franklin Lakes, NJ). Erythrocytes were lysed using ammonium chloride potassium lysis buffer (Qiagen, Tokyo, Japan). Cell suspensions were incubated with a biotinylated lineage cocktail [anti-CD5, anti-CD45R (B220), anti-CD11b, anti-Gr-1 anti-Ly-6G/C, and anti-Ter-119; 130–090-858; Miltenyi Biotec, Auburn, CA], followed by anti-biotin MicroBeads (130–090-485; Miltenyi Biotec). Lin^- cells were isolated with a MACS column and separator (Miltenyi Biotec) and stained with anti-c-Kit-APC-Cy7 (2B8; BD Biosciences), anti-Sca-1-PE-Cy7 (D7; Biolegend, San Diego, CA), anti-CD34-Alexa Flour 700 (RAM34; BD Biosciences), anti-CD135-PE (A2F10; Biolegend), or anti-OPN (18621; Immuno-Biological Laboratories, Gunma, Japan) antibody. Anti-rabbit IgG-conjugated APC (R&D Systems, Minneapolis, MN) was used as the anti-OPN secondary antibody. A DAPI solution (D523; DOJINDO, Kumamoto, Japan) was used to exclude dead cells. LSK cells were sorted first, and the LSK cells were subsequently isolated using CD135 and CD34 antibodies (Fig. 1*A*). $CD135^-$ $CD34^-$ cells were identified as LT-HSCs, $CD135^-$ $CD34^+$ cells as short-term reconstituting HSCs (ST-HSCs), and $CD135^+$ $CD34^+$ cells as multipotent hematopoietic progenitors (MPPs; Fig. 1*A*). Lin^- OPN^+ cells were identified as osteoblastic niche cells (Fig. 1*A*). After coculture experiments, the culture medium was discarded, and adherent cells were removed using Hanks' buffered saline including 0.25% trypsin and 1 mM EDTA for 15 min. Sorting of LT-HSCs and osteoblastic niche cells was carried out by FACS as described above.

Osteoblastic niche cells and LT-HSCs coculture. To investigate the interactions between LT-HSCs and osteoblastic niche cells, we cocultured sorted LT-HSCs (6×10^3 cells) and osteoblastic niche cells (6×10^4 cells) with DMEM supplemented with 10% FBS, 1% penicillin, 150 ng/ml Fms-like tyrosine kinase 3 (FLT3) ligand, 150 ng/ml stem cell factor (SCF), and 150 ng/ml TPO at the glucose concentrations of 100 mg/dl for the normal glucose medium or 450 mg/dl for the high-glucose medium. Osteoblastic niche cells and LT-HSCs were seeded at the same time in 16-well chamber slides (Thermo Scientific, Barrington, IL) at 37°C in 5% CO_2-air for 7 days. On *day 3*, the culture medium was changed. The cocultured cell morphology was observed under phase-contrast microscopy.

HSC differentiation and the colony-forming assay. To examine the hematopoiesis potential of the hematopoietic cells, LSK cells were sorted from the femora and tibiae of vehicle and STZ-injected mice by FACS and cultured in CytoSelect Methylcellulose Medium (CBA-320; Cell Biolabs) containing 10% FBS, 500-ng/ml SCF, 100-ng/ml IL-3, 100-ng/ml GM-CSF, and 30-ng/ml erythropoietin (Ep) at 5% CO_2-air and 37°C for 7 days (25). Colony formation was measured with CyQuant GR dye solution (CBA-320; Cell Biolabs). The number of sorted LSK cells was counted by FACS.

Serum TRAP5b assay. To compare the bone resorption activity of the osteoclasts in vehicle- and STZ-injected mice, blood was collected

Table 1. *Primer sequences for PCR*

Protein	Primer Sequence
N-cadherin	
F	5′-AATCAGACGGCTAGACGAGAGG-3′
R	5′-TCAGCAGATTTAAGGCCCTCAT-3′
β-Catenin	
F	5′-ACGCGTGTGAGAAAGAATACAGAC-3′
R	5′-GCTTGAGTTTGGTTCTGGGC-3′
β_1-Integrin	
F	5′-TGGAAAATTCTGCGAGTGTGAT-3′
R	5′-TGCCAGTGTAATTGGGATAGCA-3′
Wnt10b	
F	5′-GCGAAGGATAATAGCAGGCAT-3′
R	5′-TTGTCACCCGAGGTCCCATA-3′
Dkk1	
F	5′-CAAAAATGTATCACACCAAAGGACAA-3′
R	5′-TGCTTGGTACACACTTGACCT-TCTT-3′
Fzd4	
F	5′-GTGGATGCCGATGAACTGAC-3′
R	5′-ACAGCGTTCCAATCACCAAA-3′
Fzd7	
F	5′-TATCGCCTACAACCAGACCATC-3′
R	5′-GGGTGCGTACATAGAGCATAAGA-3′
LRP5	
F	5′-CCCACTCACGGGTGTCAAA-3′
R	5′-TGCTCCACTGAGCTCCCATT-3′
LRP6	
F	5′-TGGCTTGGCGGTGTGAT-3′
R	5′-CACACGGGACAATTGAGTTCA-3′
Ang-1	
F	5′-CAGCACGAAGGATGCTGATAAC-3′
R	5′-TTGTCCCGCAGTGTAGAACATT-3′
Tie2	
F	5′-AAGCATGCCCATCTGGTTAC-3′
R	5′-GCCTGCCTTCTTTCTCACAC-3′
CXCL12	
F	5′-GCTCTGCATCAGTGACGGTA-3′
R	5′-TAATTACGGGTCAATGCACA-3′
CXCR4	
F	5′-CTTTGTCATCACACTCC-CCTT-3′
R	5′-GCCCACATAGACTGCCT-TTTC-3′
TPO	
F	5′-CCAGACGGAACAGAGCAAG-3′
R	5′-CTGTCCTCGTGCTGCCAT-3′
MPL	
F	5′-CCTGCACTGGAGGGAGGTCT-3′
R	5′-GGCTCCAGCACCTTCCAGTC-3′
GAPDH	
F	5′-CTACAGCAACAGGGTGGTGGAC-3′
R	5′-GGATAGGGCCTCTCTTGCTCAG-3′

F, forward; R, reverse.